Application of Cluster Analysis to Boundary-layer Cloud Property Pairs from CERES/TRMM Measurements

Zachary A. Eitzen, SSAI, Kuan-Man Xu, and Takmeng Wong, NASA-LaRC
http://cloud-object.larc.nasa.gov

1. Cloud Object Data

The cloud object data were taken from CERES-TRMM, over Jan-Aug 1998. Each boundary-layer cloud object is a contiguous region of CERES footprints that have cloud tops below 3 km, and a cloud fraction of: 99-100% (overcast), 40-99% (stratocumulus), or 10-40% (shallow cumulus). The cloud objects in this work were all observed over the ocean, and within 30 degrees of the Equator.

2. Spearman Rank Correlations

We are not only interested in 1-D distributions of cloud properties (see Xu et al. 2007), but also how they change with one another. One way to examine this is with 2-D (joint) PDFs. However, with a large number of cloud properties, a simple correlation coefficient summarizing each pair is useful. Spearman rank correlation has the advantage of being less sensitive to outliers than the standard Pearson correlation.

Microphysical/optical cloud property pairs

Table 1: Spearman correlations (R) for satellite footprint data from overcast objects >300 km.

	τ	r_e	albedo	SW CRF
r_e	0.245			
albedo	0.919	0.153		
SW CRF	-0.869	-0.082	-0.753	
LWP	0.921	0.574	0.814	-0.752

Table 2: Spearman correlations (R) for satellite footprint data from stratocumulus objects >300 km.

	τ	r_e	albedo	SW CRF
r_e	0.316			
albedo	0.771	0.164		
SW CRF	-0.850	-0.181	-0.829	
LWP	0.920	0.638	0.677	-0.743

Table 3: Spearman correlations (R) for satellite footprints from shallow cumulus objects >150 km.

	τ	r_e	albedo	SW CRF
r_e	0.290			
albedo	0.328	-0.053		
SW CRF	-0.563	-0.083	-0.473	
LWP	0.940	0.572	0.270	-0.500

Macrophysical cloud property pairs

Table 4: Spearman correlations (R) for satellite footprints from overcast objects >300 km.

	CTT	OLR	LW CRF
OLR	0.616		
LW CRF	-0.658	-0.651	
SST	0.597	0.300	-0.131

Table 5: Spearman correlations (R) for satellite footprints from stratocumulus objects >300 km.

	CTT	OLR	LW CRF	SST
OLR	0.529			
LW CRF	-0.528	-0.594		
SST	0.730	0.422	-0.219	
cld frac	-0.119	-0.243	0.345	-0.044

Table 6: Spearman correlations (R) for satellite footprints from shallow cumulus objects >150 km.

	CTT	OLR	LW CRF	SST
OLR	0.183			
LW CRF	-0.267	-0.330		
SST	0.689	0.088	-0.025	
cld frac	-0.075	-0.080	0.211	-0.015

Mixed cloud property pairs

Table 7: Spearman correlations (R) for satellite footprints from overcast objects >300 km.

	τ	r_e	albedo	SW CRF
CTT	-0.248	-0.158	-0.339	0.275
OLR	-0.159	-0.203	-0.199	0.096
LW CRF	0.192	0.173	0.253	-0.189
SST	-0.159	0.078	-0.236	0.184

Summary

- Correlations between cloud property pairs are smaller for shallow cumulus cloud objects than for stratocumulus or overcast cloud objects.
- A slope-based cluster analysis of the relationship between τ and r_e revealed that for each cloud type, there is a cluster associated with negative slopes, one with slopes near zero, and two positive slopes. The cluster with negative slopes for overcast clouds may be associated with dust, while this does not appear to be the case for other types.
- Using W_{700}, there appear to be a moist and a dry cluster for each boundary-layer type, and the relationship between SST and OLR is roughly linear throughout the SST range for the dry cluster, while the OLR stays in a roughly constant range for the moist cluster. The sum of these clusters produces a decrease in OLR with SST for high SSTs, which has been seen in clear-sky results by Hallberg and Inamdar (1993) and others.

3. Cluster Analysis

Cloud optical depth and effective radius

Overcast cloud objects

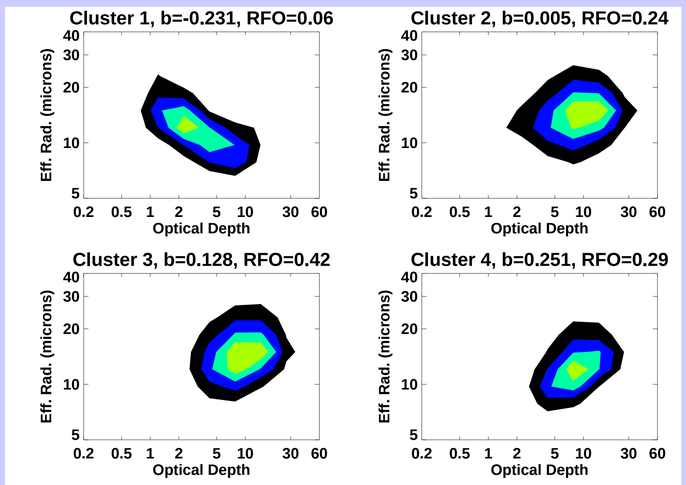

Fig. 1: Log-log contour plots of r_e and τ for clusters of overcast cloud objects, arranged in order of increasing b, which is the slope of the linear fit to ln(r_e) and ln(τ) for each cloud object. RFO is the relative frequency of occurrence for each cluster.

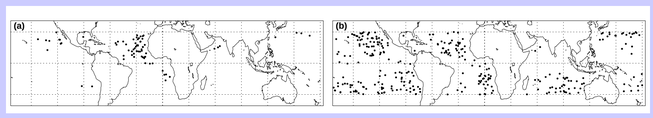

Fig. 2: Centers of the cloud objects that constituted (a) cluster 1, (b) cluster 2 from Fig. 1. Locations of clusters 3 and 4 are similar to those of cluster 2.

Stratocumulus cloud objects

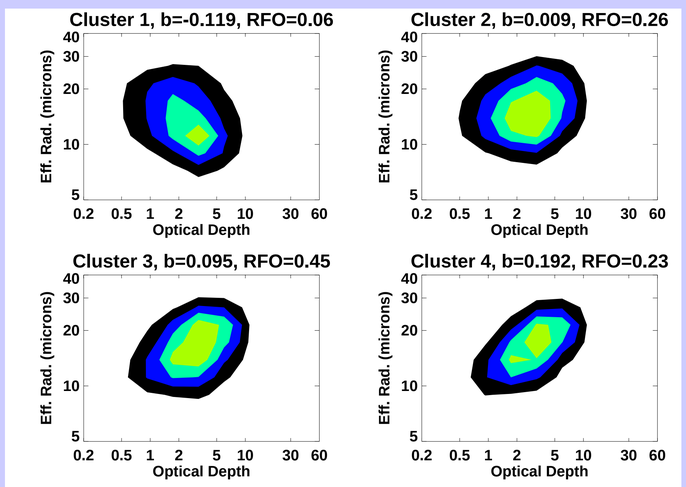

Fig. 3: As in Fig. 1, except for stratocumulus cloud objects.

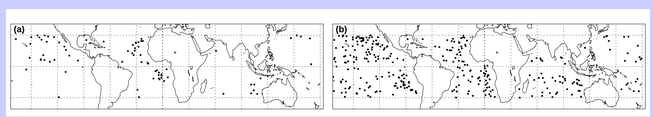

Fig. 4: Centers of the cloud objects that constituted (a) cluster 1, (b) cluster 2 from Fig. 3. Locations of clusters 3 and 4 are similar to those of cluster 2.

Shallow cumulus cloud objects

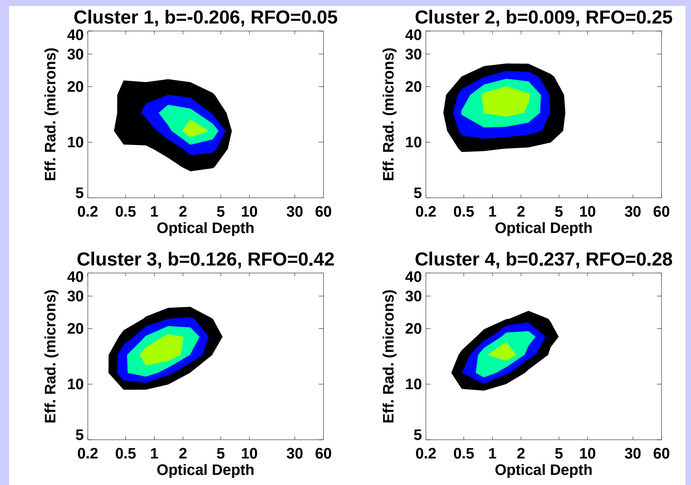

Fig. 5: As in Fig. 1, except for shallow cumulus cloud objects.

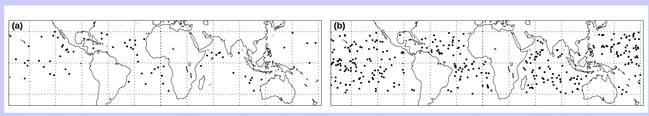

Fig. 6: Centers of the cloud objects that constituted (a) cluster 1, (b) cluster 2 from Fig. 5. Locations of clusters 3 and 4 are similar to those of cluster 2.

SST and OLR

Overcast cloud objects

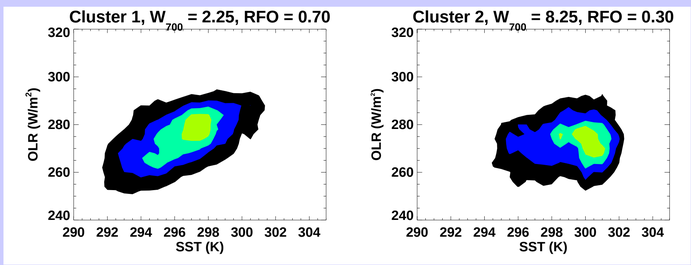

Fig. 7: Contour plots of SST and OLR for clusters of overcast cloud objects, arranged in order of increasing W_{700}, which is the average precipitable water above 700 mb for each cloud object. RFO is the relative frequency of occurrence for each cluster.

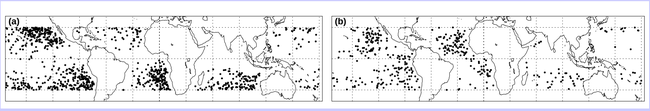

Fig. 8: Centers of the cloud objects that constituted (a) cluster 1, (b) cluster 2 from Fig. 7.

Stratocumulus cloud objects

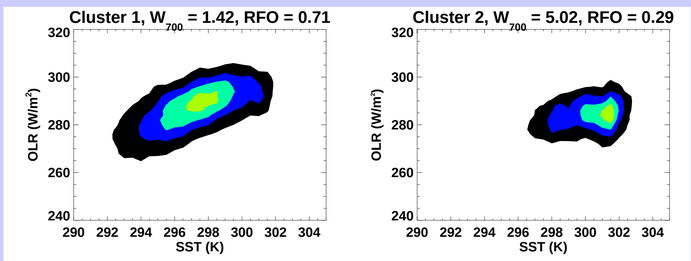

Fig. 9: As in Fig. 7, except for stratocumulus cloud objects.

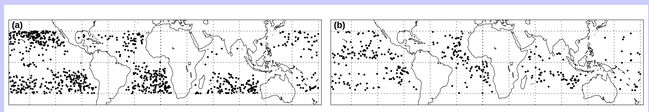

Fig. 10: Centers of the cloud objects that constituted (a) cluster 1, (b) cluster 2 from Fig. 9.

Shallow cumulus cloud objects

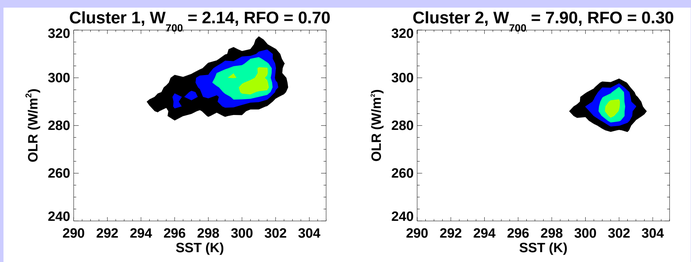

Fig. 11: As in Fig. 7, except for shallow cumulus cloud objects.

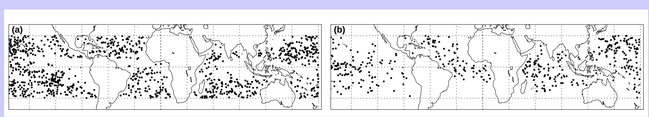

Fig. 12: Centers of the cloud objects that constituted (a) cluster 1, (b) cluster 2 from Fig. 11.

References

Hallberg, R., and A. K. Inamdar, 1993: Observations of seasonal variations in atmospheric greenhouse trapping and its enhancement at high sea surface temperature. *J. Climate,* **6,** 920-931.

Xu, K.-M., T. Wong, B. A. Wielicki, and L. Parker, 2007: Statistical analyses of cloud object data from CERES. Part IV: Boundary-layer cloud objects during 1998 El Niño. *J. Climate* (under revision).